Free-volume dynamics in glasses and supercooled liquids

John T. Bendler,[1] John J. Fontanella,[1] M. F. Shlesinger,[2] J. Bartoš,[3] O. Šauša,[4] and J. Krištiak[4]
[1]*Physics Department, U. S. Naval Academy, Annapolis, Maryland 21402, USA*
[2]*Physical Sciences Division, Office of Naval Research, 800 N. Quincy Street, Arlington, Virginia 22217, USA*
[3]*Polymer Institute of SAS, Dúbravská cesta 9, 842 36 Bratislava, Slovak Republic*
[4]*Institute of Physics of SAS, Dúbravská cesta 9, 842 28 Bratislava, Slovak Republic*
(Received 8 October 2004; revised manuscript received 27 December 2004; published 31 March 2005)

A free-volume theory is developed based on the defect diffusion model (DDM). In addition, positronium annihilation lifetime spectroscopy (PALS) ortho-positronium free-volume and intensity data are presented for poly(propylene glycol) with a molecular weight of 4000 (PPG 4000) in both the glassy and liquid states and dielectric relaxation and electrical conductivity data are reported for PPG 4000 in the liquid state. The DDM is used to interpret all of the data for PPG 4000 and previously reported PALS and dielectric relaxation data for glycerol. It is shown that while the PPG 4000 data exhibit a preference for the three-halves power law, the data for glycerol favor the first power (standard Vogel-Fulcher-Tammann) law. Good agreement between the DDM and the experimental results is found for all of the electrical data and the PALS free-volume data. While reasonable agreement is also found for the PALS intensity data for PPG 4000, a discrepancy exists between the experimental PALS intensity data and theory for glycerol. For the electrical conductivity for PPG 4000, a transition is observed at the same temperature (about $1.4T_g$ where T_g is the glass transition temperature) where the PALS free volume changes from steeply rising with temperature to approximately independent of temperature. The same behavior is observed at about $1.5T_g$ for previously reported dielectric relaxation and PALS data for glycerol. Model parameters are presented that show the dominance of mobile single defects above $(1.4–1.5)T_g$ and the dominance of immobile clustered single defects below T_g. Finally, a coherent picture of glasses and glass-forming liquids is presented based on the theory and results of the experiments.

DOI: 10.1103/PhysRevE.71.031508 PACS number(s): 64.70.Pf, 64.70.Ja, 77.22.−d, 78.70.Bj

I. INTRODUCTION

In spite of the enormous technological and scientific importance of the glassy state, a fundamental understanding of why many liquids supercool below their crystallization temperature and then solidify to an amorphous solid state remains elusive [1–5]. Most remarkably, perhaps, no consensus has yet been reached as to whether the basic physics of glass formation is controlled by kinetics or thermodynamics. The Kauzmann entropy paradox strongly suggests that the thermodynamics of the liquid state plays a major role. Kauzmann first noted that the excess heat capacity of a supercooled liquid results in such a rapid decrease in the entropy of the liquid with falling temperature that if the glass transition did not intervene, the entropy of the liquid would shortly fall below the entropy of the crystal [6]. The intervention of the kinetic glass transition to avoid this thermodynamic catastrophe is either a striking coincidence, or else evidence that underlying thermodynamic changes are fundamentally related to glass formation. Kinetic features of glass formation have been intensely studied in recent years [1] and a consensus has largely resulted. The transition to the vitreous state is accompanied by a dramatic slowing of all molecular processes in the fluid. Characteristic time scales vary from 10^{-9} to 10^{3} s over a temperature interval as small as 50 °C. Hallmarks of the region above the glass transition temperature T_g include relaxation studies that find a stretched exponential law

$$\phi(t) = \exp[-(t/\tau)^{\beta}] \tag{1}$$

with $\beta < 1$, and the time scale τ diverging with an essential singularity according to a Vogel-Fulcher-Tammann (VFT) law [7–9]

$$\tau = A \exp\left(\frac{D}{T - T_0}\right) \tag{2}$$

as temperature falls towards a value T_0. This critical temperature, where τ diverges, is below T_g, and evidence suggests that it is closely tied to the Kauzmann temperature T_K, the temperature at which the entropy of the liquid extrapolates to zero.

In previous work [10–15], a defect diffusion model (DDM) was described that is consistent with the above-mentioned kinetic features of glass-forming liquids. When the defect mean trapping time is longer than the experimental observation time the stretched exponential law follows, and the time scale is inversely related to the concentration of mobile single defects (MSDs). Immobile, clustered single defects (ICSDs) were also considered. As temperature falls the number of ICSDs increases leading to increased rigidity and giving rise to a Vogel-Fulcher-Tammann type law. Previous work [10–15] focused completely on the kinetics of the fluid and the kinetic effects of the defects. At a given temperature and pressure above T_g, the mobile defects are conserved in number and assumed to be reasonably abundant so that they can visit every site in the fluid on the time scale of the experiment. The defects catalyze events in the supercooled liquid by freeing up degrees of freedom directly par-

ticipating in a molecular process. If dielectric relaxation is studied, the pertinent degrees of freedom are dipole orientations, and the defects assist relaxation by freeing dipole rotations. The degrees of freedom associated with the defects themselves were neglected and not assumed to contribute to the changes taking place as T_g was approached or traversed.

In this paper we show that positron annihilation lifetime spectroscopy (PALS) experiments above and below T_g can be successfully interpreted if one identifies the MSDs and ICSDs with the free-volume holes in which the orthopositronium (o-Ps) resides. We can term these free-volume regions packets, since we assume that some are mobile (like the MSDs) and experience intermittent diffusion throughout the fluid visiting and relaxing dipoles, ions, volume, stress, etc., and some are fixed in position (like the ICSDs). Identifying the defects with free-volume packets yields excellent agreement with experiment both above and below T_g. The results give insight into the manner whereby the kinetics and thermodynamics of a supercooled liquid are simultaneously altered through the same defect mechanism.

Many other theories of glass-forming liquids exist and have recently been reviewed [2–4]. In addition, a theory of glass formers based on a lattice model has recently appeared [16]. To date, however, none of the theories has been applied to the results of PALS experiments both above and below T_g.

II. A MODEL OF MOBILE FREE-VOLUME PACKETS

In the DDM, the total volume of the MSDs can be written

$$V_{\mathrm{sing}}(T) = NV_{\mathrm{MSD}}c_1 \tag{3}$$

where N is the total number of sites, c_1 is the concentration of MSDs (probability that a MSD exists), and V_{MSD} is the mean volume of a MSD. Next, the total volume of the clusters is given by

$$V_{\mathrm{clus}}(T) = NV_{\mathrm{ICSD}}(c - c_1) \tag{4}$$

where c is the total concentration of single defects (probability that a single defect exists) and V_{ICSD} is the mean volume of an ICSD. ($c - c_1$ is the concentration of ICSDs.)

Next, from previous work [10–14] and generalizing to include the effect of an anisotropic correlation volume [15], the concentration of the MSDs is

$$c_1 = c\exp\left[-\left(\frac{\beta B^* T_C^{0.5\eta\gamma}}{(T-T_C)^{0.5\eta\gamma}}\right)\right], \quad T > T_C, \tag{5a}$$

and

$$c_1 = 0, \quad T < T_C. \tag{5b}$$

Further, $B^* = -(L_1L_2L_3/d_0^3)\ln(1-c)/\beta$ where β is the stretched exponential parameter, d_0 is the average distance between neighbor "lattice sites" (positions where defects can exist) at $P=0$ and some reference temperature, and L_1, L_2, and L_3 are characteristic lengths associated with the correlation volume. These lengths are defined by $\xi_i(T) = L_i[T_C/(T-T_C)]^{0.5}$. T_C is the critical temperature below which there are no MSDs and γ is a constant that describes local field effects. It has been pointed out that $\gamma=1$ except very near to T_C [15] so the approximation that $\gamma=1$ will be made in what follows. Finally, η is a constant describing the dimensionality of the correlation volume. This gives rise to the following VFT-like equation for dynamical properties:

$$x_{\mathrm{DDM}}(P,V,T) = A_x\exp\left(\frac{B^* T_C^{0.5\eta}}{(T-T_C)^{0.5\eta}(1-\delta)}\right). \tag{6}$$

x represents the dielectric relaxation time, electrical resistivity, or reciprocal viscosity, for example. In the case where $\eta=2$ and $\delta=0$ the "standard" VFT equation, Eq. (2),

$$x_{\mathrm{DDM}}(P,V,T) = A_x\exp\left(\frac{B^* T_C}{T-T_C}\right) \equiv A_x\exp\left(\frac{D}{T-T_0}\right), \tag{7}$$

is obtained and if $\eta=3$ (isotropic three dimensional correlation volume) and $\delta=0$ the theory predicts the original 3/2 power VFT-like law [10–14]

$$x_{\mathrm{DDM}}(P,V,T) = A_x\exp\left(\frac{B^* T_C^{1.5}}{(T-T_C)^{1.5}}\right). \tag{8}$$

Finally, then, the total volume of the defects (total free volume in the material) is given by

$$V_{\mathrm{defect\ total}} = V_{\mathrm{sing}} + V_{\mathrm{clus}}. \tag{9}$$

This theory of free volume can be compared with other free-volume theories that have been used widely [17–20].

III. EXPERIMENTS AND RESULTS

The poly(propylene glycol) of molecular weight 4000 (PPG 4000) studied in the present work was obtained from Polysciences, Inc. The PALS data for glycerol have been reported previously [21].

A. Positron annihilation lifetime spectroscopy

The PALS spectra for PPG 4000 were obtained by the conventional fast-fast coincidence method using plastic scintillators coupled to Philips XP 2020 photomultiplier tubes. The time resolution full width at half maximum of the prompt spectra was 320 ps. A standard three component analysis was carried out using a PATFIT-88 software package [22].

The temperature range of measurement was 15–320 K. For data from 15 to 300 K, the sample was placed at the end of the cold finger of a closed cycle helium refrigerator. The sample was in vacuum and the temperature was controlled to within ±0.5 K during the data acquisition. For measurements from 290 to 320 K, the samples were placed in a sample holder at atmospheric pressure and the temperature was controlled to within ±2 K.

The sample was initially cooled to 15 K in about 2 h and data were taken after allowing the sample to achieve thermal equilibrium. The sample temperature was then increased several kelvin, allowed to equilibrate for 15 min, and data were taken. The process of increasing the sample temperature, allowing the sample to equilibrate in 15 min, followed by data acquisition was repeated until the highest temperature was achieved. In all cases, the measuring time was 2 h or longer.

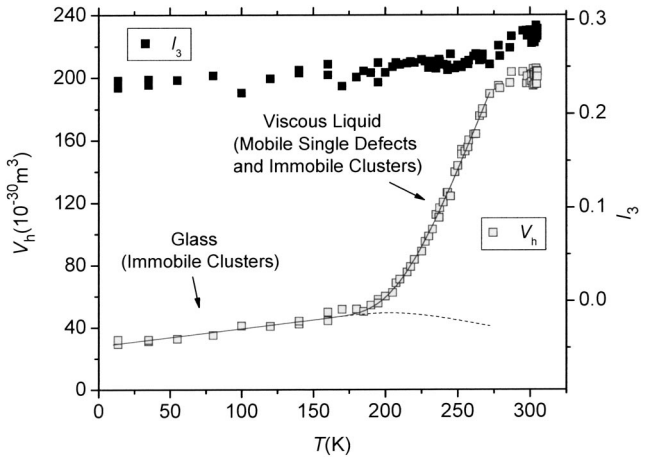

FIG. 1. PALS hole volume V_h (open symbols) and relative o-Ps intensity I_3 (solid symbols) vs temperature for PPG 4000. The solid line is the best-fit curve [Eq. (19)] based on the defect diffusion model with $\eta=3$ and $\bar{N}=2$. The curved dashed line is the volume associated with clusters above T_g.

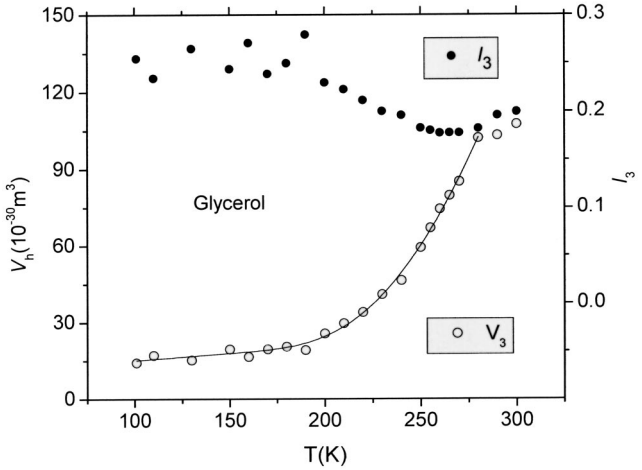

FIG. 2. PALS hole volume V_h, (open symbols) vs temperature for glycerol. The solid line is the best-fit curve [Eq. (19)] based on the defect diffusion model with $\eta=2$ and $\bar{N}=2$.

After the heating cycle, data were taken similarly during a cooling cycle beginning at room temperature. No hysteresis was observed.

The resultant values of the o-Ps lifetime τ_3 were related to the average radius of a spherical free-volume hole with an electron layer of thickness ΔR using

$$\tau_3 = \frac{1}{2}\left[1 - \frac{R_h}{R_0} + \frac{1}{2\pi}\sin\left(\frac{2\pi R_h}{R_0}\right)\right]^{-1} \tag{10}$$

which is based on a simple quantum-mechanical model [23]. $R_0 = R_h + \Delta R$ where R_h is the radius of a spherical free-volume hole and ΔR has been determined from the experimental values of τ_3 for molecular solids of known hole size to be $\Delta R = 1.66 \times 10^{-10}$ m. Finally, the volume of the free-volume holes was calculated using $V_h = (4\pi R_h^3/3)$. The relative intensity I_3, which reflects the PALS free-volume population density [24], was also determined from the data. The PALS results for V_h and I_3 vs temperature for PPG 4000 are shown in Fig. 1. The PALS results for glycerol [21] are shown in Fig. 2.

For both PPG 4000 and glycerol at the lowest temperatures the PALS volumes exhibit an approximately linear region with a small positive slope. At about T_g for each material (197 K for PPG 4000 and 190 K for glycerol), the PALS volumes begin to increase rapidly and nonlinearly as temperature increases. At about 272 K for PPG 4000 and 280 K for glycerol, the rapid rise in the PALS volume with temperature ceases and at higher temperatures the PALS volume is relatively independent of temperature. This behavior is similar to that observed for other materials [25–27].

B. Dielectric relaxation and electrical conductivity

The electrical measurements were carried out using either a CGA-85 capacitance measuring assembly, which operates at 17 frequencies from 10 to 10^5 Hz, or a Solartron 1296 interfaced with a Solartron 1255 frequency response analyzer, which was used over the frequency range from about 10^{-2} to 10^6 Hz. All measurements were recorded as G/ω where G is the conductance and ω is the angular frequency. The temperature was varied in a Precision Cryogenics CT-14 Dewar and the temperature was controlled using a Lake-Shore Cryotronics DR92 temperature controller. The conductivity at temperatures other than room temperature and all of the dielectric relaxation data were determined using a cell similar to that described elsewhere [28].

Electrical response typical of both the α relaxation and ionic conductivity were observed. For convenience, the imaginary part of a Havriliak-Negami (HN) function [29]

$$\varepsilon''(\omega) = \mathrm{Im}\left\{\frac{\Delta\varepsilon_\alpha}{[1 + (i\omega\tau_{\mathrm{HN}})^{\alpha_1}]^{\gamma_1}}\right\} \tag{11}$$

was best fitted to the imaginary part of the dielectric constant in order to determine the peak position for the α relaxation.

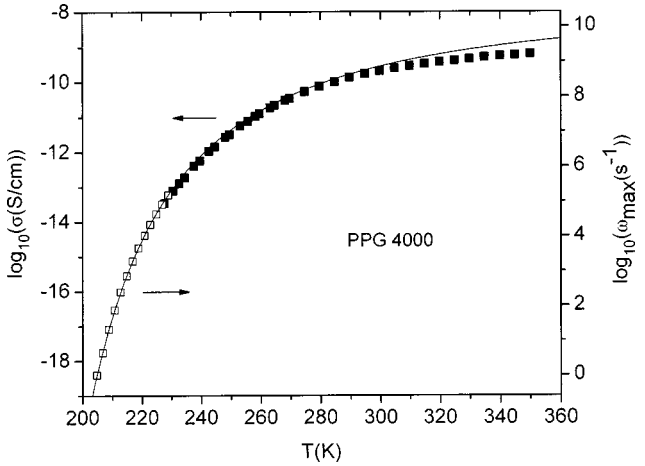

FIG. 3. Logarithm of the frequency of the maximum value of the best-fit HN function, $\omega_{\max}$ (open symbols), and logarithm of the electrical conductivity σ (solid symbols) vs temperature for the α relaxation in PPG 4000. The solid line is the best-fit 3/2 power law [Eq. (8)] to the dielectric relaxation data.

TABLE I. Best-fit parameters for VFT-like equations applied to PALS, dielectric relaxation, and electrical conductivity data for PPG 4000. The PALS parameters are for $\overline{N}=2$. χ^2 are reduced values as given by ORIGIN®.

First power (VFT)					Three halves power			
PALS								
	$V_{MSD,0}$ (10^{-30} m^3)	$\beta B^* T_C$ (K)	T_C (K)	χ^2	$V_{MSD,0}$ (10^{-30} m^3)	$\beta B^* T_C^{1.5}$ (K$^{1.5}$)	T_C (K)	χ^2
	324±44	273±34	140±7	7.2	238±25	3310±520	118±8	6.9
Electrical conductivity (present work)								
Temperature (K)	$\log_{10}[A_\sigma$ (S K/cm)]	B^*	T_C (K)	χ^2	$\log_{10}[A_\sigma$ (S K/cm)]	B^*	T_C (K)	χ^2
227.5–269.6	−3.69±0.13	5.95±0.32	168.8±1.6	0.00017	−4.63±0.10	5.55±0.39	150.0±1.9	0.00014
Dielectric relaxation								
Temperature (K)	$\log_{10}[A_\tau$ (s)]	B^*	T_C (K)	χ^2	$\log_{10}[A_\tau$ (s)]	B^*	T_C (K)	χ^2
Present work								
204.8–228.8	12.4±0.2	5.5±0.2	171.5±0.7	0.00025	10.8±0.13	3.6±0.2	160.8±0.9	0.00021
Schönhals and Schlosser [30]								
195.7–268.2	12.2±0.2	7.2±0.3	163.4±0.8	0.0091	10.7±0.14	5.5±0.3	150.1±1.1	0.0084
Park *et al.* [31]								
210.5–268	11.9±0.4	4.9±0.7	173±3	0.0116	10.9±0.3	3.8±0.7	159±3.9	0.0110
Leon *et al.* [32]								
196–232.5	11.6±0.4	5.2±0.5	170±1.4	0.0101	10.0±0.3	3.1±0.4	161±1.8	0.0095
Schwartz *et al.* [33]								
205–268	12.44±0.03	5.65±0.05	172.9±0.2	0.00018	11.17±0.05	4.1±0.1	159.9±0.5	0.00066

The quantities $\Delta\varepsilon_\alpha$, τ_{HN}, α_1, and γ_1 are the fitting parameters. The resultant peak position vs temperature is shown by the open symbols in Fig. 3.

Both Eqs. (7) and (8) were best fitted to the relaxation time vs temperature data for the α relaxation. The curve generated by the best-fit 3/2 power VFT-like equation is shown by the solid line in Fig. 3. For comparison, those equations were also best fitted to data published by several authors [30–33]. All of the fitting parameters for PPG 4000 are listed in Table I. Fits of Eqs. (7) and (8) were also made to literature data for glycerol [34–38]. Those parameters are listed in Table II along with VFT parameters from the literature [39]. It is noted that, on the basis of χ^2, four of the five sets of dielectric relaxation data for PPG 4000 favor the 3/2 power law while all of the dielectric relaxation data for glycerol favor the first power (VFT) law.

The conductivity measurement at room temperature for PPG 4000 was carried out in a cylindrical cell identical to that used in the study of ion-containing PPG [40]. The conductance was determined from an impedance arc at room temperature and the conductivity was calculated using

$$\sigma = \frac{Gl}{A} \tag{12}$$

where l and A are the length and area of the sample, respectively. The conductivity at room temperature was found to be 1.7×10^{-10} S/cm. Since the conductivity is very low for PPG 4000, it was only possible to obtain an impedance arc for the highest temperatures studied. Consequently, the conductance was calculated from G/ω at 0.1 Hz for all temperatures other than room temperature and it was assumed that the relative change in conductivity is the same as the relative change in conductance.

The results for the conductivity vs temperature for PPG 4000 are shown by the filled symbols in Fig. 3. The axes have been shifted so that both types of data appear to form a single curve. Equations (7) and (8) with a factor of $1/T$ in the preexponential because of the Nernst-Einstein relation [13] were best fitted to the data for comparison with the dielectric relaxation results. The best-fit parameters are listed in Table I. As for most of the dielectric relaxation data, the fit favors the 3/2 power law. It is seen in Fig. 3 that the curve generated by the 3/2 power VFT-like equation for the α relaxation also does a reasonable job of representing the low temperature portion of the electrical conductivity data. This is not surprising since it has been known for many years that both the α relaxation and the conductivity appear to be related [41]. However, the best-fit curve begins to deviate from the conductivity data in the vicinity of 270 °C.

To further investigate the difference between the best-fit curve and the data, a Stickel plot [42] was made for both the conductivity and dielectric relaxation data for PPG 4000 and is shown in Fig. 4. The conductivity shows an abrupt change

TABLE II. Best-fit parameters for VFT-like equations applied to PALS and dielectric relaxation data for glycerol. The PALS parameters are for $\overline{N}=2$. χ^2 are reduced values as given by ORIGIN®.

	First power (VFT)				Three halves power			
			PALS					
	$V_{MSD,0}$ (10^{-30} m^3)	$\beta B^* T_C$ (K)	T_C (K)	χ^2	$V_{MSD,0}$ (10^{-30} m^3)	$\beta B^* T_C^{1.5}$ (K$^{1.5}$)	T_C (K)	χ^2
	430±230	570±170	107±23	2.58	240±99	8100±2900	72±28	2.60
			Dielectric relaxation					
Temperature (K)	$\log_{10}[A_\tau$ (s)]	B^*	T_C (K)	χ^2	$\log_{10}[A_\tau$ (s)]	B^*	T_C (K)	χ^2
			Lunkenheimer *et al.* [34]					
185–273	15.1±0.4	18.1±1.6	128.0±2.7	0.0082	13.2±0.4	23.3±3.5	106.2±4.0	0.0107
			Stickel *et al.* [35]					
186.9–280.5	15.12±0.02	19.5±0.1	125.9±0.2	0.00009	13.28±0.03	26.6±0.3	102.8±0.3	0.00019
			Kudlich *et al.* [36]					
185–278	15.1±0.3	18.6±1.4	129.2±2.3	0.0117	13.2±0.3	23.8±2.7	107.4±3.0	0.0125
			Davidson and Cole [37], McDuffie and Litovitz [38]					
198.6–265.6	15.3±0.1	20.3±0.7	126.0±1.1	0.00022	13.5±0.1	28.8±1.7	101.7±1.7	0.00032
			Jeong *et al.* [39]					
200–270	15.2	17.9	129					

in slope at about 270 K which is approximately the temperature where the best-fit curve begins to deviate from the conductivity data. This implies the existence of a change in the liquid (presumably a liquid-liquid transition) at about 270 K. This transition occurs at about the same temperature as the high temperature transition in the PALS data for PPG 4000.

It is also interesting that, even though the axes have not been shifted, the conductivity and dielectric relaxation data fall on the same, approximately straight-line segment at low temperatures. This agreement between the α relaxation and the electrical conductivity data represents further evidence for a common origin of the two processes.

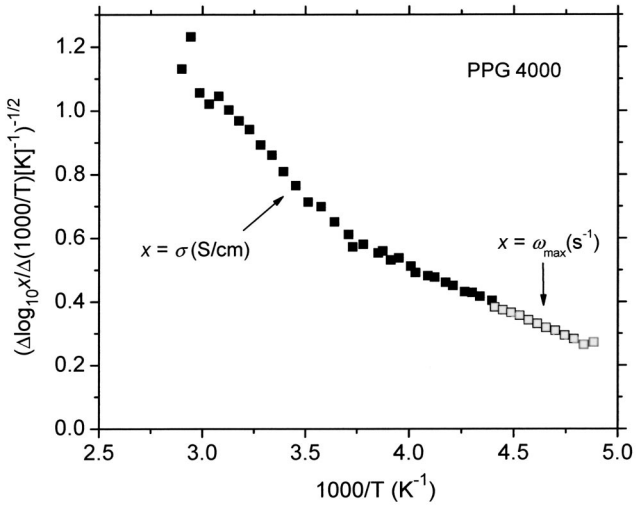

FIG. 4. Stickel plot for the electrical conductivity and frequency of the maximum value of the HN function for PPG 4000.

IV. ANALYSIS OF THE FREE-VOLUME DATA

The theory was applied to the PALS data as follows. The assumption is made that at low temperatures ($T<T_C$) only clusters exist ($c_1=0$). Consequently, at low temperatures, the PALS free volume is a measure of the average size of a free volume cluster from which it follows that

$$V_{\mathrm{PALS}}^{\mathrm{LT}} = \overline{N} V_{\mathrm{ICSD}} \tag{13}$$

where $\overline{N}$ is the average number of single defects associated with a cluster.

The ICSDs are assumed to have a thermal expansion coefficient α_{ICSD}. If $V_{\mathrm{ICSD},0}$ is the volume of an ICSD at $T=0$ K, then

$$V_{\mathrm{PALS}}^{\mathrm{LT}} = \overline{N} V_{\mathrm{ICSD},0}(1+\alpha_{\mathrm{ICSD}} T). \tag{14}$$

This equation was fitted to the data for PPG 4000 below 160 K where the concentration of MSDs is very small or zero. The result for PPG 4000 is that $\overline{N}V_{\mathrm{ICSD},0}=28.1\times10^{-30}$ m^3 and $\alpha_{\mathrm{ICSD}}=4.0\times10^{-3}$ K^{-1}. Since the data are approximately linear, for glycerol Eq. (14) was fitted to the data over the temperature range 101–190 K. The fitting parameters for glycerol are $\overline{N}V_{\mathrm{ICSD},0}=9.6\times10^{-30}$ m^3 and $\alpha_{\mathrm{ICSD}}=5.8\times10^{-3}$ K^{-1}.

The next assumption that is made is that above T_C both MSDs and ICSDs exist. In this case, the PALS free volume is

$$V_{\mathrm{PALS}}^{\mathrm{HT}} = V_{\mathrm{defect\ total}}/N_{\mathrm{defects}} \tag{15}$$

where $V_{\mathrm{defect\ total}}$ is given by Eq. (9) and N_{defects} is the total number of defects. However, because some of the single defects are clustered, the total number of defects is given by

$$N_{\text{defects}} = \frac{N(c - c_1)}{\overline{N}} + Nc_1. \tag{16}$$

Consequently, it is predicted that

$$V_{\text{PALS}}^{\text{HT}} = \frac{c_1 V_{\text{MSD}} + (c - c_1) V_{\text{ICSD}}}{(c - c_1)/\overline{N} + c_1} \tag{17}$$

and it follows that

$$V_{\text{PALS}}^{\text{HT}} = \frac{V_{\text{MSD}} \exp\left[-\left(\frac{\beta B^* T_C^{0.5\eta}}{(T - T_C)^{0.5\eta}}\right)\right] + V_{\text{ICSD}}\left\{1 - \exp\left[-\left(\frac{\beta B^* T_C^{0.5\eta}}{(T - T_C)^{0.5\eta}}\right)\right]\right\}}{\exp\left[-\left(\frac{\beta B^* T_C^{0.5\eta}}{(T - T_C)^{0.5\eta}}\right)\right] + \frac{1}{\overline{N}}\left\{1 - \exp\left[-\left(\frac{\beta B^* T_C^{0.5\eta}}{(T - T_C)^{0.5\eta}}\right)\right]\right\}} \quad T > T_C. \tag{18}$$

Equivalently, the working equation is

$$V_{\text{PALS}}^{\text{HT}} = \frac{(\overline{N} V_{\text{MSD}} - V_{\text{PALS}}^{\text{LT}}) \exp\left[-\left(\frac{\beta B^* T_C^{0.5\eta}}{(T - T_C)^{0.5\eta}}\right)\right] + V_{\text{PALS}}^{\text{LT}}}{1 + (\overline{N} - 1)\exp\left[-\left(\frac{\beta B^* T_C^{0.5\eta}}{(T - T_C)^{0.5\eta}}\right)\right]}. \tag{19}$$

In order to fit the free-volume data, the simplest cluster was chosen by assuming that on average there are two single defects per cluster, i.e., $\overline{N}=2$. It was also assumed that MSDs exhibit the same thermal expansion behavior as do the ICSDs, i.e., it was assumed that $\alpha_{\text{MSD}}=\alpha_{\text{ICSD}}$, so that

$$V_{\text{MSD}} = V_{\text{MSD},0}(1 + \alpha_{\text{ICSD}} T). \tag{20}$$

A best fit was carried out and the resulting fitting parameters are listed in Tables I and II for PPG 4000 and glycerol, respectively, and the best-fit curves are shown in Figs. 1 and 2. It is clear that the fit is good for both materials except at high temperatures. It is interesting that, on the basis of χ^2, the 3/2 power law provides a better fit for PPG 4000 while the first power law provides a better fit for glycerol. This is consistent with the fits to the dielectric relaxation and electrical conductivity data.

V. DISCUSSION

The preference of all of the glycerol data for the first power (standard VFT) law and the preference of most of the PPG 4000 data for the three halves power law can be understood in terms of the DDM. As mentioned in Sec. II, and discussed previously [15], the three halves power law of Eq. (8) describes isotropic correlation volumes ($\eta=3$) while the first power law Eq. (7) corresponds to an anisotropic correlation volume ($\eta=2$). Consequently, the conclusion is that glycerol exhibits a strongly anisotropic correlation volume. This is consistent with the strong (directional) hydrogen bonding that occurs in glycerol. Correspondingly, PPG 4000 appears to exhibit isotropic (nondirectional) van der Waals intermolecular bonding.

The present treatment of PALS data gives an account of the free volume both in the liquid near T_g and in the glass below T_g. PALS data are usually interpreted in terms of a single type of hole which expands rapidly at temperatures above T_g. However, a reason for this rapid expansion has never been satisfactorily established. The present theory offers an interpretation of PALS data suggesting that the o-Ps spends time in two types of free-volume packets, with the population of the larger packets growing rapidly above T_C. In this picture, the terms in the numerator of Eq. (18) have a simple interpretation. Specifically, the term $\exp\{-[\beta B^* T_C^{0.5\eta}/(T-T)_C^{0.5\eta}]\}=P$ is proportional to the probability that o-Ps is associated with a MSD and $(1-P)$ is proportional to the probability that o-Ps is associated with a cluster.

This interpretation is reminiscent of the explanation given by Kobayashi *et al.* [24] to account for the single, well-defined mean lifetime that is usually observed by PALS experiments. Specifically, while it is expected that there is a wide distribution of sizes of free-volume holes, the data can be characterized by a single mean lifetime. The explanation given by Kobayashi *et al.* [24] is that averaging takes place because o-Ps can exist in more than one hole before annihilation. Such averaging will take place if o-Ps can visit both clusters and mobile single defects before annihilation. This is consistent with our theory since above T_C the MSDs are in thermal equilibrium with ICSDs.

Several other aspects of the theory are consistent with the PALS data. First, the relative intensity I_3 is proportional to the number *density* of holes [24] and thus should be proportional to the total number of defects, N_{defects}, as given by Eq. (16), and also inversely proportional to the volume. At low temperatures $T<T_C$, $c_1=0$ and c, N, and $\overline{N}$ are constant so that N_{defects} is constant. Since the change in volume with temperature is small for the glass, it is predicted that I_3 is approximately constant at low temperatures. At high temperatures $T>T_C$, N_{defects} increases as temperature increases. The reason is that, in the present model, two single defects are generated when one cluster breaks up as temperature increases and thus a (small) increase in I_3 with temperature above T_g is predicted. In addition, the volume increases as temperature increases. Consequently, I_3 will either increase

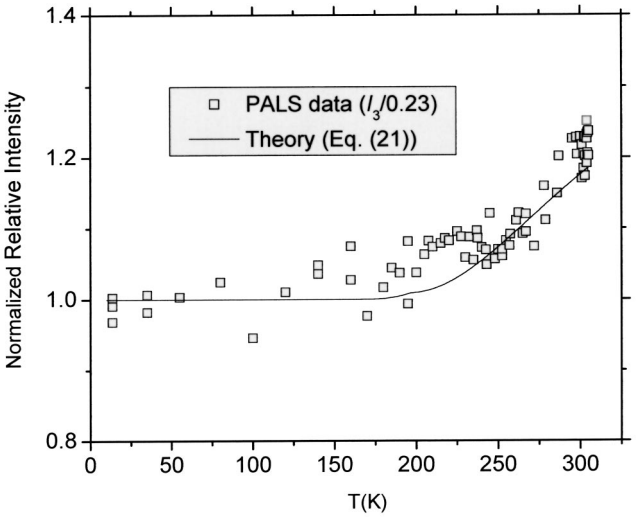

FIG. 5. Normalized relative intensity vs temperature for PPG 4000. The data are shown by the points and the theory based on the three halves power law and Eq. (21) is shown by the line.

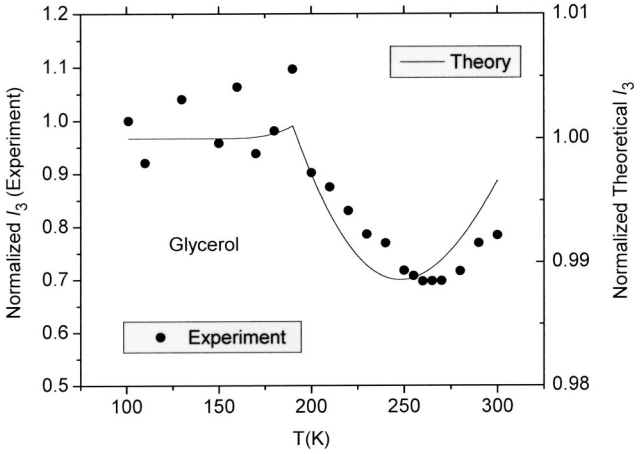

FIG. 6. Normalized relative intensity vs temperature for glycerol. The data are shown by the points and the theory based on the first power law and Eq. (21) is shown by the line.

or decrease as temperature increases depending upon whether N_{defects} or the volume dominates the temperature dependence. In order to undertake a quantitative test of the model, the following quantity was identified as the theoretical normalized relative intensity:

$$\frac{\overline{NN}_{\text{defects}}}{Nc(V_{\text{macro}}/V_{\text{macro},T_g})} = \frac{(c-c_1)/c + \overline{Nc}_1/c}{1+\alpha(T-T_g)}, \qquad (21)$$

where α is the macroscopic thermal expansion coefficient, V_{macro} is the macroscopic volume at any temperature, and V_{macro,T_g} is the macroscopic volume at T_g. For glycerol, α is taken to be 5.0×10^{-4} K^{-1} which is the average of the value quoted by Kovacs [43] and the value calculated from the data given by Piccirelli and Litovitz [44]. The value used for PPG 4000 is $\alpha=6.97\times10^{-4}$ K^{-1} [45]. The experimental data were normalized by arbitrarily dividing I_3 by 0.235 for PPG and 0.255 for glycerol, the respective low temperature limiting values of I_3. The theoretical and experimental normalized relative intensities are shown in Figs. 5 and 6. For PPG 4000, the approximately constant value below T_g is reproduced and both the theoretical and experimental relative intensities show an increase of about 20% as temperature increases from T_g (197 K) to T_{b2} (272 K). (See below for discussion of T_{b2}.) Interestingly, the theory also does a reasonable job of predicting the variation of intensity above T_{b2} as can be seen in Fig. 5 since both the experiment and theory are plotted up to 305 K. For glycerol, the approximately constant value below T_g is reproduced. In Fig. 6, above T_g, I_3 decreases monotonically until it reaches a minimum, after which I_3 increases monotonically. However, because the theoretical and experimental values of I_3 are on different scales, the magnitude of the theoretical decrease just above T_g is much smaller than is observed experimentally. This is not surprising since there are phenomena that affect the intensity but not the lifetime. However, the reason for the difference between the theoretical and experimental intensities for glycerol remains to be determined.

Next, the values of the exponents such as $\beta B^* T_C$ are of interest. The general features of the PALS exponent are consistent with those for the electrical data in that the values for PPG 4000 are smaller than for glycerol. This is usually interpreted as an indication that PPG 4000 is more "fragile" than glycerol. In fact, in early work, the value $D=B^*T_C$ was proposed to be a measure of "fragility" [46–48]; the smaller the value of D, the more "fragile" the material. However, in order to make a detailed comparison of the exponents, some care must be taken since the numerator of the exponent for PALS is $\beta B^* T_C^{0.5\eta}$ vs $B^* T_C^{0.5\eta}$ for either dielectric relaxation or electrical conductivity. Interestingly, this makes the present theory of PALS independent of the stretched exponential parameter since B^* has β in the denominator, i.e., $B^*=-(L_1L_2L_3/d_0^3)\ln(1-c)/\beta$. Using the values of T_C and $\beta=0.51$ for PPG 4000 [49–52], B^* was calculated for the PPG 4000 PALS data and the results are listed in Table III. The value of β for glycerol, however, appears to be temperature dependent, varying from about 0.55 at T_g to about 0.8 at

TABLE III. PALS parameters.

	First power (VFT)					Three halves power				
Compound	B^*	c_1/c	$V_{\text{sing}}/V_{\text{defect total}}$	$(c-c_1)/c$	$V_{\text{clus}}/V_{\text{defect total}}$	B^*	c_1/c	$V_{\text{sing}}/V_{\text{defect total}}$	$(c-c_1)/c$	$V_{\text{clus}}/V_{\text{defect total}}$
		T_{b2}	T_{b2}	T_g	T_g		T_{b2}	T_{b2}	T_g	T_g
PPG 4000	3.8	0.12	0.76	0.9937	0.87	5.1	0.18	0.79	0.9909	0.86
Glycerol	9.7–6.7	0.036	0.77	0.9990	0.92	24.1–16.6	0.068	0.78	0.9982	0.92

about 280 K [53]. That leads to the values for the PALS B^* that are listed in Table III.

While the value of B^* is about the same for both PALS and the electrical data for the three halves power law, the PALS values are smaller for the first power (standard VFT) law. Since the three halves power law provides a better fit for most of the data for PPG 4000, the exponents for the PALS and dynamical data are probably about the same. However, for glycerol, for which all of the data favor the first power law, the value of B^* is significantly smaller for the PALS data than for the dynamical data. Certainly, differences between the characteristic parameters for the PALS and dynamical data are not unexpected since it is likely that the PALS response is sensitive to more defects than just those responsible for either dielectric relaxation or electrical conductivity, for example. The concept is that MSDs exist that are not involved in dielectric relaxation or electrical conductivity and PALS should also be sensitive to those MSDs.

This interpretation may also explain the behavior of the critical temperature T_C. Again, as is clear from Tables I and II, the general trend observed for the PALS critical temperature is the same as that for the electrical data since the critical temperatures for the PALS data for glycerol are significantly lower than those observed for PPG 4000. However, it is also clear from Tables I and II that there is a tendency for T_C to be lower for the PALS data than for the dynamical data though the critical temperatures are almost the same to within the uncertainty for glycerol. Again, the explanation is that PALS is a measure of all MSDs while the dynamical data are only sensitive to a subset. That implies that, on average, the concentration of MSDs becomes zero (MSDs cease to exist) at a lower temperature than the dielectric relaxation or electrical conductivity MSDs.

Next, in the standard VFT formulation, it is found that the volume of a MSD extrapolated to zero temperature, $V_{\mathrm{MSD},0}$, is approximately 273×10^{-30} m^3 for PPG 4000 and 570×10^{-30} m^3 for glycerol. These values are somewhat larger than the values based on the 3/2 power law and can be compared with the van der Waals volume of a monomer unit of PPG 4000, 61×10^{-30} m^3 and the van der Waals volume of a molecule of glycerol, 86.5×10^{-30} m^3. The corresponding radii, which are on the order of 0.4 nm, are reasonable and consistent with what would be expected to facilitate dynamical processes such as dipole reorientation or ion transport. A noteworthy feature is that for both materials the value of $V_{\mathrm{MSD},0}$ is larger than the volume of a cluster since $\overline{N}V_{\mathrm{ICSD},0}=28.1\times10^{-30}$ m^3 for PPG 4000 and $\overline{N}V_{\mathrm{ICSD},0}=9.6\times10^{-30}$ m^3 for glycerol. At first sight, this may seem unreasonable and it would be for a cluster of atoms. However, in the present theory these are empty holes and the concept is that when the holes cluster, the atoms fit together more efficiently so that there is a reduction in the free volume.

Next, in the case of PPG 4000, as has been pointed out from both the electrical conductivity (Fig. 3) and PALS, a transition occurs at about 272 K. For glycerol, the PALS data exhibit a transition at about 280 K. Correspondingly, dielectric relaxation data for glycerol show a transition at about 285 K [48]. The ratio of the transition temperature to T_g is approximately 1.47 for glycerol and 1.38 for PPG 4000. Evidence for subtle transitions at temperatures above the glass transition temperature, usually but not always close to $1.2T_g$, has been discussed in detail as early as 1963 [54]. In fact, Boyer discussed the evidence for a transition in glycerol at $1.48T_g$. Boyer labeled this transition temperature as T_{LL}, reflecting the fact that he considered this to be a liquid-liquid transition. Transitions in this temperature regime have also been discussed by van Krevelen [55] and Stickel *et al.* [56]. Stickel *et al.* label the transition temperature as T_B. In the case of the PALS data, the temperature where this transition occurs is often labeled as T_{b2} [57] and interpreted as a limitation of the PALS technique. The reason is that above T_{b2} the holes can no longer be considered to be static and τ_3 becomes approximately constant because of the effect on the o-Ps of the vibrations of the atoms near the holes.

Some insight into the nature of this transition can be obtained by examining the model parameters at T_{b2} (272 K for PPG 4000 and 280 K for glycerol). The values of c_1/c, the ratio of the average concentration of MSDs to the average total concentration of defects, and $V_{\mathrm{sing}}/V_{\mathrm{defect\ total}}$, the ratio of the average volume of MSDs to the average total volume of defects, were calculated and the results are listed in Table III. The values of c_1/c for PPG 4000 (0.12 and 0.18 for the first power and three halves power laws, respectively) are in the range of fractions that are typical for percolation [58,59] but the values for glycerol (0.036 and 0.068) are lower. However, it is also seen in Table III that $V_{\mathrm{sing}}/V_{\mathrm{defect\ total}}$ is about the same for both materials and both laws near T_{b2}, ranging from about 0.76 to 0.79. Consequently, at T_{b2} on the order of 78% of the total defect volume is mobile single defects. The large fractional volume of MSDs at T_{b2} is reasonable and is qualitatively consistent with the results of recent computer modeling studies of PPG 4000 which suggest that at about 20 K above T_{b2}, free volume percolates [60]. It is interesting to speculate that a true liquid ($T>T_{b2}$) is a liquid where MSDs percolate.

The theory parameters at T_g are also of interest since, in the context of defect diffusion theory, the glass transition temperature is interpreted to be the temperature at which rigidity percolates [10–13]. The values of $(c-c_1)/c$, the ratio of the average concentration of ICSDs to the average total concentration of defects, and $V_{\mathrm{clus}}/V_{\mathrm{defect\ total}}$, the ratio of the average volume of ICSDs to the average total volume of defects, at T_g (197 K for PPG 4000 and 190 K for glycerol) were calculated and the results are listed in Table III. For PPG 4000 it is found that $(c-c_1)/c=0.9937$ and 0.9909 for the first power and three halves power laws, respectively, while for glycerol, the values are 0.9990 and 0.9982. While those values are larger than would be expected for standard percolation phenomena, it is also found that $V_{\mathrm{sing}}/V_{\mathrm{defect\ total}}$ is 0.87 for the first power law and 0.86 for the three halves power law for PPG 4000 and about 0.92 in both cases for glycerol. Consequently, the volume fraction of ICSDs at T_g is on the order of the volume fraction of MDSs at T_{b2}. Thus, the data are qualitatively consistent with the defect diffusion interpretation that the glass transition occurs when rigidity percolates.

VI. SUMMARY

In summary, a free-volume theory is developed based on the DDM. PALS o-Ps free-volume and intensity data are pre-

sented for PPG 4000 in both the glassy and liquid states. In addition, dielectric relaxation and electrical conductivity data are reported for PPG 4000 in the liquid state. The DDM is used to interpret all of the data for PPG 4000 and previously reported PALS data for glycerol.

It is shown that while the PPG data exhibit a preference for the three halves power law, the data for glycerol favor the first power (standard VFT) law. Good agreement between the DDM and the experimental results is found for all of the electrical data and the PALS free-volume data. In general, both the value of the exponent and the critical temperature in the VFT-like law are found to be lower for the PALS data than for the electrical data. The difference is attributed to a PALS experiment being sensitive to all types of defects (free-volume holes), while the electrical experiments only sample a rather specialized subset of defects. While good agreement is also found for the PALS intensity data for PPG 4000, a discrepancy exists between the experimental PALS intensity data and theory for glycerol.

For the electrical conductivity for PPG 4000, a transition is observed at the same temperature (approximately $1.4T_g$) where the PALS free volume changes from steeply rising with temperature to approximately independent of temperature. The same behavior is observed for previously reported dielectric relaxation and PALS data for glycerol. Model parameters are presented that show the dominance of MSDs above $1.4T_g$ and the dominance of ICSDs below T_g.

As a consequence, the following picture of glasses and glass-forming liquids emerges.

(1) Below T_g a material is dominated by immobile clusters and thus a glass is a material where rigidity percolates. There may also be mobile defects in the glassy state such as those responsible for the β relaxation. Presumably, those defects do not cluster since the β relaxation in the glassy state usually exhibits Arrhenius behavior [61] and the DDM predicts Arrhenius behavior for nonclustering defects [15]. However, these sub-T_g defects have not been taken into account in the present simple formulation.

(2) Between T_g and a higher temperature such as $1.4T_g$ (T_B, T_{b2}, or T_{LL}) there is a mixed system of MSDs and ICSDs. Depending on the system and correspondingly the behavior of the defects, there may be transitions or changes in dynamics at an intermediate temperature. For example, in some materials, PALS data show changes at T_{b1} that is intermediate between T_g and T_{b2} [57].

(3) Above the higher temperature, a material is dominated by mobile defects and thus a true liquid is one where MSDs percolate. It is interesting to speculate that above the higher temperature is the region where mode coupling theory (MCT) is applicable [62–64]. The fact that the higher temperature region begins well above T_g would explain the reason that the critical temperature in the MCT is significantly above T_g.

ACKNOWLEDGMENTS

This work was supported in part by NSF Grant No. 0217129 (J.B., J.J.F., and J.T.B.), VEGA Grants No. 2/3026/23 (J.B.) and No. 2/4103/24 (J.K.), APVT Grant No. 51-045302 (J.K. and J.B.), and the Office of Naval Research (J.J.F.). In addition, J.T.B. gratefully acknowledges support from the Department of Defense Army Research Office (Grant No. DAAD19-01-1-0482).

[1] Proceedings of the Fourth International Discussion Meeting on Relaxations in Complex Systems, edited by K. L. Ngai [J. Non-Cryst. Solids **307–310,** 1 (2002)].
[2] C. A. Angell, Science **267**, 1924 (1995).
[3] P. G. Debenedetti and F. H. Stillinger, Nature (London) **410**, 259 (2001).
[4] F. Ritort and P. Sollich, Adv. Phys. **52**, 219 (2003).
[5] K. L. Ngai, L. Bao, A. F. Yee, and C. L. Soles, Phys. Rev. Lett. **87**, 215901 (2001).
[6] W. Kauzmann, Chem. Rev. (Washington, D.C.) **43**, 219 (1948).
[7] H. Vogel, Phys. Z. **22**, 645 (1921).
[8] G. S. Fulcher, J. Am. Ceram. Soc. **77**, 3701 (1925).
[9] G. Tammann and W. Hesse, Z. Anorg. Allg. Chem. **156**, 245 (1926).
[10] J. T. Bendler and M. F. Shlesinger, J. Mol. Liq. **36**, 37 (1987).
[11] J. T. Bendler and M. F. Shlesinger, J. Stat. Phys. **53**, 531 (1988).
[12] J. T. Bendler and M. F. Shlesinger, Nucl. Phys. **5**, 82 (1988).
[13] J. T. Bendler, J. J. Fontanella, and M. F. Shlesinger, Phys. Rev. Lett. **87**, 195503 (2001).
[14] J. T. Bendler, J. J. Fontanella, and M. F. Shlesinger, J. Chem. Phys. **118**, 6713 (2003).
[15] J. T. Bendler, J. J. Fontanella, M. F. Shlesinger, and M. C. Wintersgill, Electrochim. Acta **49**, 5249 (2004).
[16] J. P. Garrahan and D. Chandler, Proc. Natl. Acad. Sci. U.S.A. **100**, 9710 (2003).
[17] M. H. Cohen and D. Turnbull, J. Chem. Phys. **31**, 1164 (1959); **34**, 120 (1961); **52**, 3038 (1970).
[18] M. H. Cohen and G. S. Grest, Phys. Rev. B **20**, 1077 (1979); Adv. Chem. Phys. **48**, 455 (1981).
[19] P. B. Macedo and T. A. Litovitz, J. Chem. Phys. **42**, 245 (1965).
[20] R. Simha and T. Somcynsky, Macromolecules **2**, 342 (1969); L. A. Utracki and R. Simha, Macromol. Theory Simul. **10**, 17 (2001).
[21] J. Bartoš, O. Šauša, J. Krištiak, T. Blochowicz, and E. Rossler, J. Phys.: Condens. Matter **13**, 11473 (2001).
[22] J. Krištiak, J. Bartoš, K. Krištiaková, O. Šauša, and P. Bandzuch, Phys. Rev. B **49**, 6601 (1994).
[23] S. Tao, J. Chem. Phys. **56**, 5499 (1972); M. Eldrup, D. Lightbody, and J. N. Sherwood, Chem. Phys. **63**, 51 (1981); H. Nakanishi, Y. C. Jean, and S. J. Wang, in *Positron Annihilation Studies of Fluids*, edited by S. C. Sharma (World Scientific, Singapore, 1988) p. 292.
[24] Y. Kobayashi, W. Zheng, E. F. Meyer, J. D. McGervey, A. M.

Jamieson, and R. Simha, Macromolecules **22**, 2302 (1989).
[25] J. R. Stevens, S. H. Chung, P. Horoyski, and K. R. Jeffrey, J. Non-Cryst. Solids **172–174**, 1207 (1994).
[26] D. Bamford, G. Dlubek, A. Reiche, M. A. Alam, W. Meyer, P. Galvosas, and F. Rittig, J. Chem. Phys. **115**, 7260 (2001).
[27] D. Bamford, A. Reiche, G. Dlubek, F. Alloin, J.-Y. Sanchez, and M. A. Alam, J. Chem. Phys. **118**, 9420 (2003).
[28] H. W. Starkweather Jr., P. Avakian, R. R. Matheson Jr., J. J. Fontanella, and M. C. Wintersgill, Macromolecules **25**, 1475 (1992).
[29] S. Havriliak and S. Negami, J. Polym. Sci., Part C: Polym. Symp. **14**, 99 (1966).
[30] A. Schönhals and E. Schlosser, Phys. Scr., T **49**, 233 (1993).
[31] I. S. Park, K. Saruta, and S. Kojima, J. Therm Anal. Calorim. **57**, 687 (1999).
[32] C. Leon, K. L. Ngai, and M. Roland, J. Chem. Phys. **110**, 11 585 (1999).
[33] G. A. Schwartz, R. Bergman, and J. Swenson, J. Chem. Phys. **120**, 5736 (2004).
[34] P. Lunkenheimer, A. Pimenov, M. Dressel, Yu. G. Goncharov, R. Bohmer, and A. Loidl, Phys. Rev. Lett. **77**, 318 (1996).
[35] F. Stickel, E. W. Fischer, and R. Richert, J. Chem. Phys. **102**, 6251 (1995).
[36] A. Kudlich, S. Benkhof, T. Blochowicz, T. Tschirwitz, and E. Rossler, J. Mol. Liq. **479**, 201 (1999).
[37] D. W. Davidson and R. H. Cole, J. Chem. Phys. **19**, 1984 (1952) (discussed in Ref. [24]).
[38] G. E. McDuffie Jr. and T. A. Litovitz, J. Chem. Phys. **37**, 1699 (1962).
[39] Y. H. Jeong, S. R. Nagel, and S. Bhattacharya, Phys. Rev. A **34**, 602 (1986).
[40] J. J. Fontanella, J. Chem. Phys. **111**, 7103 (1999).
[41] R. M. Fuoss, J. Am. Chem. Soc. **63**, 369 (1941); **63**, 378 (1941).
[42] F. Stickel, E. W. Fischer, and R. Richert, J. Chem. Phys. **102**, 6251 (1995).
[43] A. Kovacs, Fortschr. Hochpolym.-Forsch. **3**, 394 (1963).
[44] R. Piccirelli and T. A. Litovitz, J. Acoust. Soc. Am. **29**, 1009 (1957).
[45] C. M. Roland, T. Psurek, S. Pawlus, and M. Paluch, J. Polym. Sci., Part B: Polym. Phys. **41**, 3047 (2003).
[46] C. A. Angell, in *Relaxations in Complex Systems* edited by K. L. Ngai and G. B. Wright (NRL, Washington, D.C., 1985), p. 3.
[47] R. Bohmer, K. L. Ngai, C. A. Angell, and D. J. Plazek, J. Chem. Phys. **99**, 4201 (1993).
[48] P. Lunkenheimer, U. Schneider, R. Brand, and A. Loidl, Contemp. Phys. **41**, 15 (2000).
[49] S. P. Andersson and O. Andersson, Macromolecules **31**, 2999 (1998).
[50] G. Williams, D. C. Watts, S. B. Dev, and A. M. North, Trans. Faraday Soc. **67**, 1323 (1971).
[51] T. Alper, A. J. Barlow, and R. W. Gray, Polymer **17**, 665 (1976).
[52] J. J. Fontanella, J. J. Wilson, M. K. Smith, M. C. Wintersgill, C. S. Coughlin, P. Mazaud, S. G. Greenbaum, and R. L. Siddon, Solid State Ionics **50**, 259 (1992).
[53] P. Lunkenheimer, A. Pimenov, B. Schiener, R. Bohmer, and A. Loidl, Europhys. Lett. **33**, 611 (1999).
[54] R. F. Boyer, Rubber Chem. Technol. **36**, 1303 (1963).
[55] D. W. van Krevelen, Angew. Makromol. Chem. **52**, 101 (1976).
[56] F. Stickel, E. W. Fischer, and R. Richert, J. Chem. Phys. **104**, 2043 (1996).
[57] J. Bartos, O. Sausa, P. Bandzuch, J. Zrubcova, and J. Kristiak, J. Non-Cryst. Solids **307–310**, 417 (2002).
[58] R. Zallen, *The Physics of Amorphous Solids* (Wiley, New York, 1983).
[59] S. Kirkpatrick, Rev. Mod. Phys. **45**, 574 (1973).
[60] D. Račko and J. Bartoš (unpublished).
[61] N. G. McCrum, B. E. Read, and G. Williams, *Anelastic and Dielectric Effects in Polymeric Solids* (Wiley, New York, 1967).
[62] U. Bengtzelius, W. Goetze, and A. Sjolander, J. Phys. C **17**, 5915 (1984).
[63] E. Leutheusser, Phys. Rev. A **29**, 2765 (1984).
[64] W. Gotze, Z. Phys. B: Condens. Matter **60**, 195 (1985).